

This item is the archived peer-reviewed author-version of:

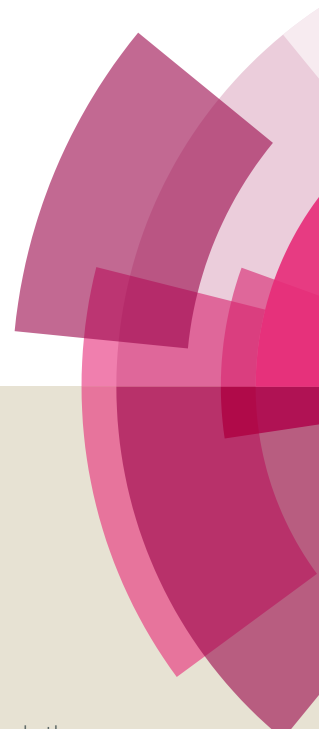
Pushing the limits of applicability of REBCO coated conductor films through fine chemical tuning and nanoengineering of inclusions

Reference:

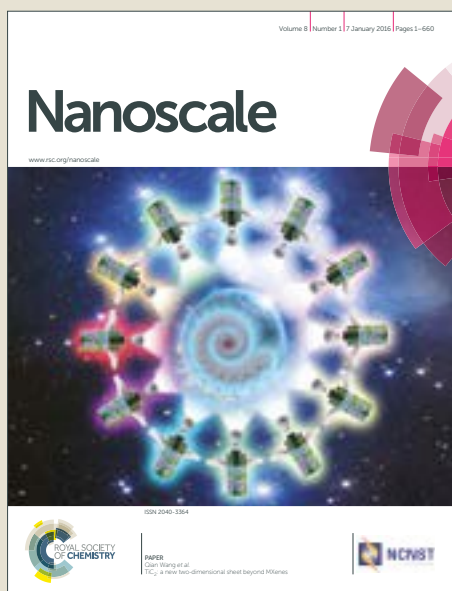
Rizzo F., Augieri A., Kursumovic A., Bianchetti M., Opherden L., Sieger M., Huehne R., Haenisch J., Meledin Alexander, Van Tendeloo Gustaaf,- Pushing the limits of applicability of REBCO coated conductor films through fine chemical tuning and nanoengineering of inclusions
Nanoscale / Royal Society of Chemistry [London] - ISSN 2040-3364 - 10:17(2018), p. 8187-8195
Full text (Publisher's DOI): <https://doi.org/10.1039/C7NR09428K>
To cite this reference: <https://hdl.handle.net/10067/1515200151162165141>

Nanoscale

Accepted Manuscript



This article can be cited before page numbers have been issued, to do this please use: F. Rizzo, A. Augieri, A. Kursumovic, M. Bianchetti, L. Opherden, M. Sieger, R. Hühne, J. Hänisch, A. Meledin, G. Van Tendeloo, J. MacManus-Driscoll and G. Celentano, *Nanoscale*, 2018, DOI: 10.1039/C7NR09428K.



This is an Accepted Manuscript, which has been through the Royal Society of Chemistry peer review process and has been accepted for publication.

Accepted Manuscripts are published online shortly after acceptance, before technical editing, formatting and proof reading. Using this free service, authors can make their results available to the community, in citable form, before we publish the edited article. We will replace this Accepted Manuscript with the edited and formatted Advance Article as soon as it is available.

You can find more information about Accepted Manuscripts in the [author guidelines](#).

Please note that technical editing may introduce minor changes to the text and/or graphics, which may alter content. The journal's standard [Terms & Conditions](#) and the ethical guidelines, outlined in our [author and reviewer resource centre](#), still apply. In no event shall the Royal Society of Chemistry be held responsible for any errors or omissions in this Accepted Manuscript or any consequences arising from the use of any information it contains.

Pushing the Limits of Applicability of REBCO Coated Conductor Films Through Fine Chemical Tuning and Nanoengineering of Inclusions

F. Rizzo ^a, A. Augieri ^a, A. Kursumovic ^b, M. Bianchetti ^b, L. Opherden ^{cd}, M. Sieger ^c, R. Hühne ^c, J. Hänisch ^{ce}, A. Meledin ^{fg}, G. Van Tendeloo ^g, J.L. MacManus-Driscoll ^b, G. Celentano ^a

^a), ENEA, Frascati Research Centre, Via E. Fermi, 45 – 00044 Frascati, Italy

^b), University of Cambridge, Department of Materials Science and Metallurgy, 27 Charles Babbage Rd., Cambridge, CB3 0FS, U.K.

^c), IFW Dresden, Institute for Metallic Materials, Helmholtzstraße 20, 01069 Dresden, Germany

^d), HZDR, High Magnetic Field Laboratory, Bautzner Landstraße 400, 01328 Dresden, Germany

^e), KIT, Institute for Technical Physics, Hermann-von-Helmholtz-Platz 1, 76344 Eggenstein-Leopoldshafen, Germany

^f), RWTH Aachen University, Central Facility for Electron Microscopy (GFE) Aachen, Germany

^g), University of Antwerp, EMAT Research Group, Groenenborgerlaan 171, 2020 Antwerp, Belgium

Abstract

An outstanding current carrying performance (namely critical current density, J_c) over a broad temperature range of 10-77 K for magnetic fields up to 12 T is reported for films of $\text{YBa}_2\text{Cu}_3\text{O}_{7-x}$ with $\text{Ba}_2\text{Y}(\text{Nb,Ta})\text{O}_6$ inclusion pinning centres (YBCO-BYNTO) and thickness in the range 220 – 500 nm. J_c values of 10 MA/cm² were measured at 30 K - 5 T and 10 K - 9 T with a corresponding maximum of the pinning force density at 10 K close to 1 TN/m³.

The system is very flexible regarding property and microstructure tuning, and the growth window for achieving a particular microstructure is wide, which is very important for industrial processing. Hence, the dependence of J_c on magnetic field angle was readily controlled by fine tuning the pinning microstructure. Transmission electron microscopy (TEM) analysis highlighted that higher growth rates induce more splayed and denser BYNTO nanocolumns with a matching field as high as 5.2 T. Correspondingly, a strong peak at $B \parallel c$ -axis is noticed when the density of vortices is lower than the nanocolumn density. YBCO-BYNTO is a very robust and reproducible composite system for high-current coated conductors over an extended range of magnetic field and temperature.

Introduction

The need for large-scale electric power applications is continuously increasing. High-temperature superconductors (HTS) are expected to successfully meet this need. Coated conductors based on biaxially textured $REBa_2Cu_3O_{7-x}$ (RE : Rare Earths) films provide a promising opportunity to develop practical HTS conductors for power applications [1]. An important step to high-current conductors was achieved when it was demonstrated the positive effect of incorporating $BaZrO_3$ (BZO) nanoparticles within YBCO for introducing flux pinning centres. This was first observed in sintered body YBCO samples [2] and then in YBCO film demonstrating that inclusion of nano-size BZO secondary phases, ranging in size from 5 nm to 100 nm with a modal particle size of 10 nm incorporated into the YBCO film matrix deposited on $SrTiO_3$ substrates, provides a factor of 5 improvement in critical current density [3]. After that, the strain-driven self-assembly process to result in BZO nanocolumns within the matrix of YBCO film for coated conductors was reported [4]. Since then, similar effects have been achieved with many other artificial pinning centres (APCs) introduced with all the deposition techniques currently used for HTS tape production [5, 6]. In recent years, coated conductors have been successfully tested in transmission cables, motors, cables for fusion or high energy physics magnets, and in other electric devices [7, 8, 9]. However, in view of commercial applications, further improvement of YBCO-based coated conductor performance over the whole ranges of magnetic field (H) and temperature (T) is needed.

Several nanoscale pinning structures have been considered in order to maximize the critical current density in different regions of temperature and magnetic field and to improve its angular behaviour. The use of self-assembled pyrochlore nanocolumns of rare earth tantalates was proposed by Harrington et al. [10]. Rare-earth tantalates, RE_3TaO_7 , with pyrochlore structure were added to YBCO and shown to result in effective pinning centres. However, it is clear from later studies by others [11] that the pyrochlore phase is not stable and in fact the double perovskite, $Ba_2RE(Nb,Ta)O_6$ forms. In the meantime, self-assembly of c -axis-oriented double perovskite nanocolumns with Ta [12] and Nb [13] was explained by the large lattice mismatch with YBCO, and large pinning forces by these nanocolumns were indeed achieved with Ba_2YTaO_6 (BYTO) and Ba_2YNbO_6 (BYNO) [12, 14, 15]. In fact, the diameter of these columns (~ 10 nm) is comparable with the YBCO coherence length, allowing a strong vortex pinning effect as H is aligned to the nanocolumns. This reflects in both an in-field J_c improvement and in the appearance of a pronounced correlated peak in J_c as a function of the magnetic field orientation, when H is close to parallel to the YBCO c -axis. As expected, the

detailed pinning behaviour is strongly affected by spacing, length, splay and linearity of the nanocolumns. This can be finely controlled by film deposition conditions (mainly deposition temperature and growth rate) [16, 17, 18].

More recently, it has been realized that the simultaneous addition of BYTO and BYNO (BYNTO) with additional rare earth oxide (via excess rare-earth composition of the matrix) leads to a nanostructure consisting of self-aligned, continuous niobate/tantalate nanorods, segmented by randomly distributed rare-earth oxide nanoparticles. Overall, the J_c performance at 77 K and in intermediate field regime up to 4 – 5 T [19, 20] as well as at 30 K for fields up to 9 T [20] is greatly improved. At 77 K, a plateau-like $J_c(B||c)$ dependence is observed over a wide magnetic field range and is ascribed to a matching between the magnetic vortices and the BYNTO columns (each column pins a single vortex), clearly indicating the effectiveness of this pinning system [20, 21].

In this work, the vortex pinning behaviour of $\text{Ba}_2\text{YTaO}_6 + \text{Ba}_2\text{YNbO}_6$ addition (YBCO-BYNTO films) is investigated in detail down to lower temperatures (< 30 K) and higher fields (up to 12 T) than previously reported. This regime is pertinent to MRI, fusion, superconducting magnetic energy storage (SMES), and generators. However, it is little understood so far. Neither is there sufficient understanding of the required optimum pinning centres (beyond them being finer and denser) nor of the materials engineering needed to create them. Furthermore, in order to explore the potential for industrial processability, where it is critical to be able to grow high-performance samples under a wide range of conditions reproducibly and reliably, samples were made in different labs under different conditions, even with slightly differing Nb:Ta ratios in the BYNTO pinning additive. Very consistent J_c performance and film microstructure were found for the films grown in the different labs. This is contrary to YBCO- BaZrO_3 (YBCO-BZO) films, where rather narrow processing conditions are required to give the same J_c performance [22]. Also, for the first time BYNTO is proven to be very effective in both intermediate and high magnetic field regimes across the whole temperature range. The J_c values exceeded those measured on YBCO-BZO at 77 K, and the difference with YBCO-BZO performance further increases with decreasing temperature. J_c values as high as 10 MA/cm² were measured at 30 K - 5 T, and 10 K - 9 T. These values are about 2-3 times larger than the J_c values reported for YBCO-BZO films under similar conditions. Hence, for the first time we show that BYNTO pinning additions are very beneficial at 30 K and below, a regime which is crucial for many HTS applications.

Results and discussion

In order to investigate the robustness of the YBCO-BYNT0 PLD growth process, we compared samples grown in three different laboratories (ENEA, Institut für Festkörper- und Werkstofforschung (IFW) and University of Cambridge (UCAM)) by PLD under a range of conditions, i.e. laser repetition rates in the range 1-10 Hz, deposition temperatures between 780 °C and 840 °C, and different BYNT0 compositions in terms of the Nb:Ta ratio. **Table 1** compares the different processing parameters used by the three groups. All samples showed T_c values of 90 K \pm 1.5 K.

	ENEA	IFW	UCAM
T_d (°C)	840	840	780
ν_L (nm)	308	248	248
f_L (Hz)	10	1	2
ρ (nm/s)	0.3	0.1	0.2
ρ_p (nm/pulse)	0.03	0.1	0.1
W (nm)	220	260	500

Table 1: Deposition temperature (T_d), laser wavelength (ν_L), laser repetition rate (f_L), growth rate (ρ), growth rate per laser pulse (ρ_p) and film thickness (W) for the different laboratories. All samples had a 5 mol.% BYNT0 addition to YBCO. The ENEA and IFW BYNT0 composition had a Nb:Ta ratio of 1:1, and the UCAM BYNT0 composition was 0.75:0.25.

The lower growth rate per pulse observed in the ENEA YBCO-BYNT0 film is due to the dependence of the target absorption coefficient α_T . For fixed laser density, α_T increases by increasing laser wavelength ν_L , and thus the energy acting in the target vaporization decreases, lowering the growth rate per pulse [23].

The J_c behaviour of an ENEA-grown YBCO-BYNT0 film with thickness of 220 nm in a wide range of temperature and applied magnetic field is shown in **Fig. 1**. At 77 K, J_c exhibits a power law decrease ($J_c \propto H^{-\alpha}$) in the low field region with the value of α lower than 0.5 ($\alpha = 0.3$), as typically reported in presence of correlated pinning defects in the YBCO matrix [4, 24]. At intermediate fields, a remarkable plateau up to about 4 – 5 T can be observed. The maximum of the pinning force density $F_p = J_c \times B$ ($B = \mu_0 H$) is reached at 4 T with $F_p^{\text{Max}} = 11.5$ GN/m³ and comparable with best values obtained in YBCO films with single-perovskite and other APCs [4, 17, 24]. In addition, practical J_c values can be sustained even in high magnetic field as shown by the high irreversibility field, B_{irr} , above 11 T (estimated with the criterion $F_p(B_{\text{irr}}) = F_p^{\text{Max}}/100$) representing one of the largest values ever reported at 77 K, cf. [3, 16, 20, 26].

The parameter α stays more or less constant as the temperature is decreased. This implies that in the whole temperature range investigated the same vortex pinning mechanisms are active in the low-to-mid magnetic field regime. Considering that the value $\alpha \sim 0.3$ is related to the presence of nanocolumnar structures being the reason for improved pinning properties [17], a temperature-independent α indicates that BYNTO remains very effective in the temperature range $T = [30 - 77]$ K. The corresponding α values, evaluated by linear fits in double logarithmic representations of the field range where $J_c \propto H^{-\alpha}$, are reported in **Table 2** for all sets of measured $J_c(H)$. While α is relatively constant, the magnitude of J_c strikingly increases, showing values greater than 10 MA/cm² up to almost 10 T at 10 K. The corresponding F_p (**Table 2** and inset of **Fig. 1**) reaches the outstanding value of 0.9 TN/m³ at 12 T (the maximum experimental achievable magnetic field in our labs). The F_p value at 30 K is almost constant and close to its maximum value of about 470 GN/m³ over the field range from 7 T to 12 T. Similar low-temperature behaviour has been previously observed only for heavily (15 - 25 at %) MOCVD deposited Zr-doped $REBa_2Cu_3O_{7-x}$ ($RE =$ rare earth) films [27] or in extremely high magnetic fields [28, 29]. The pinning landscape in that system is complex because Ba is taken from $REBa_2Cu_3O_{7-x}$ to form BZO by reaction with the added Zr. This leads to a range of other secondary defects which are hard to quantify and potentially hard to control. On the other hand, the YBCO matrix composition is not modified by the addition of 5 mol% BYNTO since it does not react with the YBCO. A significant further improvement of transport properties at low temperatures and high fields would be expected for considering higher levels of BYNTO addition. A well-defined and clean pinning would be achieved, providing precise understanding of pinning in the regime of high fields and low temperatures which is lacking at present.

However, a recent work revealed that similar performances can be achieved even with PLD YBCO - BZO films with medium doping level (2 - 4 vol.% BZO), showing pinning force densities which reach 1.5 TN/m³ at 5 K and 9 T [30].

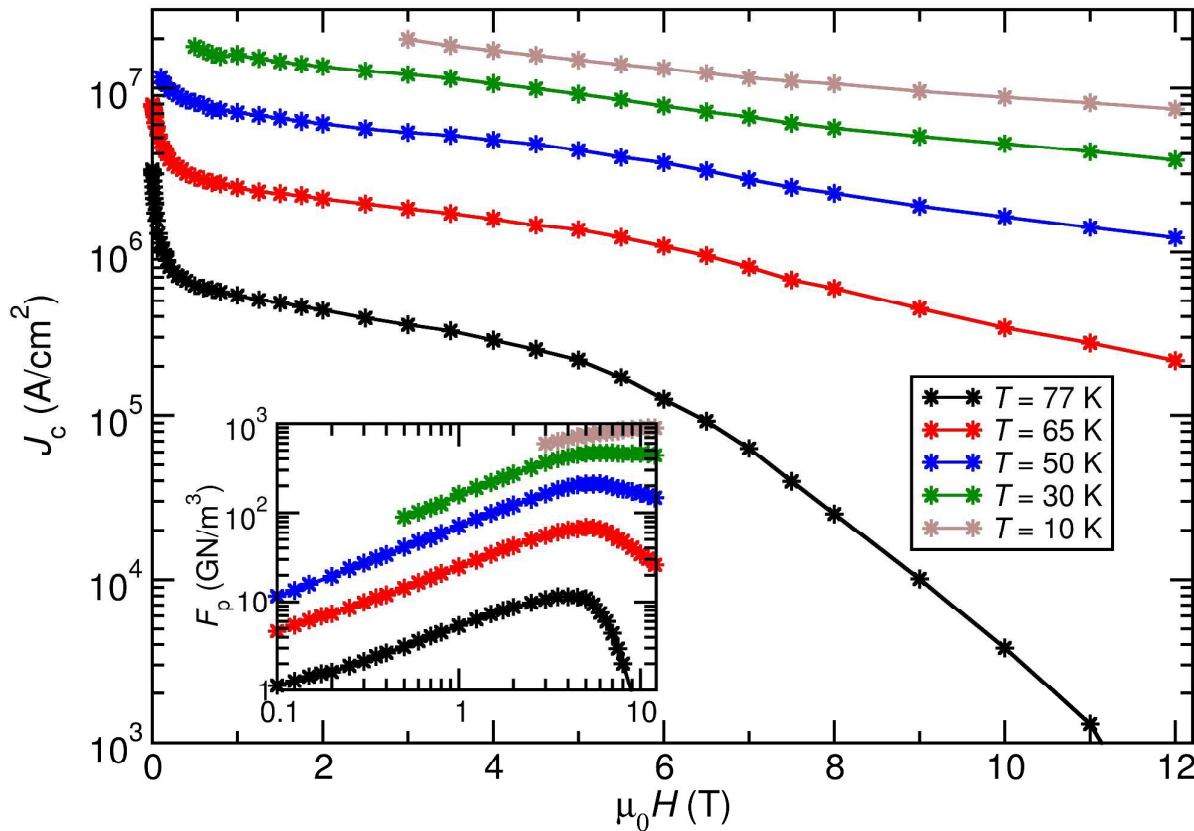


Figure 1: Dependence of the critical current density J_c on the applied magnetic field up to 12 T ($B||c$) of the ENEA YBCO-BYNT0 film in the temperature range [10 - 77] K and corresponding pinning force densities $F_p(B)$ (inset). The slopes of these F_p curves correspond to $1-\alpha$.

Temperature	77 K	65 K	50 K	30 K	10 K
α	0.30	0.24	0.21	0.26	---
$F_p^{\text{Max}}(\text{GN/m}^3)$	11.5	68.7	210.5	468.6	895*
$B(\text{T}) @ F_p^{\text{Max}}$	4	5	6	7	11 - 12

Table 2: α values, maximum pinning force density F_p^{Max} , and corresponding magnetic field of the ENEA YBCO-BYNT0 film in the whole temperature interval studied. * F_p^{Max} at 10 K is still not reached, the value reported corresponds to the maximum experimentally achievable.

Fig. 2 compares the best J_c vs B data up to 5 T at $T = 77$ K of IFW (blue circles), UCAM (red diamonds) and ENEA (black stars). For UCAM, the 75:25 BYNO:BYTO composition showed a slightly improved performance over the 50:50 composition. The samples from the different groups were grown at different repetition rates f_L ($f_L = 1$ Hz IFW, $f_L = 2$ Hz UCAM, $f_L = 10$ Hz ENEA), corresponding growth rates are given in Table 1. Film thickness ranged from 220 to 500 nm, as specified in Table 1. For reference, high-quality YBCO-BZO nanocomposite films grown with $\rho = 0.22 - 0.25$ nm/s (green squares - Ref. 14) and with $\rho = 0.16$ nm/s (orange triangles - ENEA, $f_L = 10$ Hz) on SrTiO_3 single crystal are also reported.

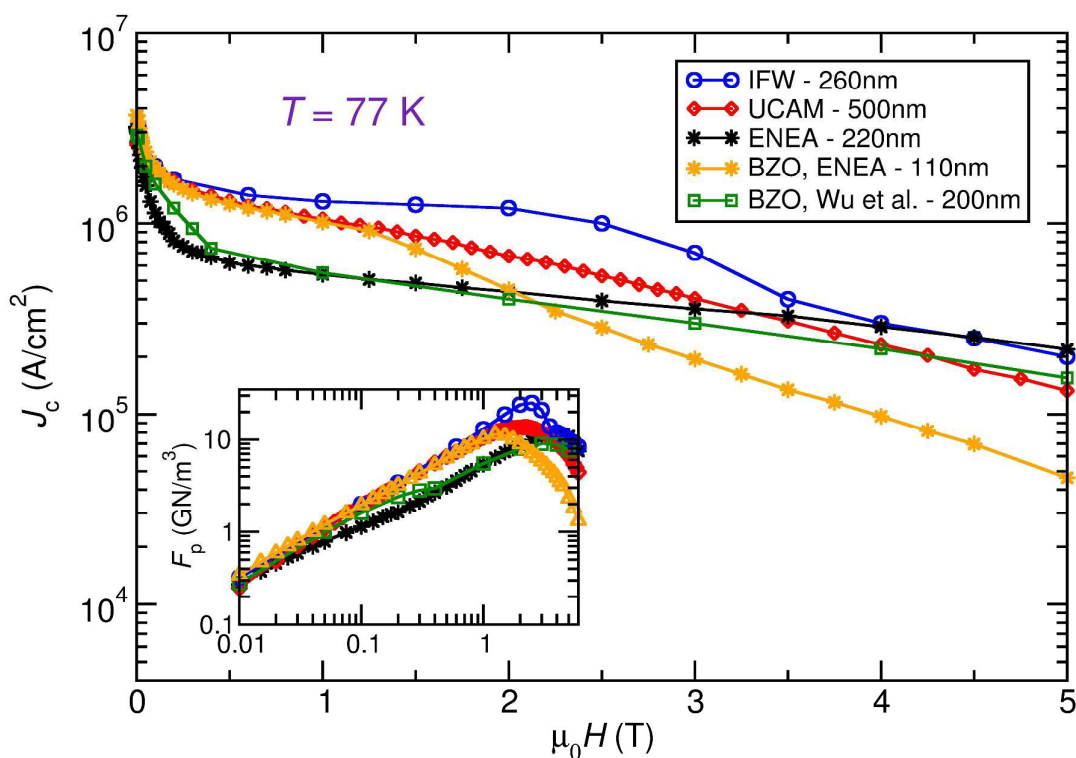


Figure 2: Comparison of the magnetic field dependence of the critical current density at $T = 77$ K for $B||c$ of YBCO-BYNTO grown by different groups, IFW (blue circles), UCAM (red diamonds) and ENEA (black stars), as well as high-quality YBCO-BZO films (Wu et al. [17] green squares and ENEA orange triangles). Inset: corresponding pinning force densities $F_p(B)$.

As **Fig. 2** clearly shows, all YBCO films with BYNTO artificial pinning centres exhibit very good in-field transport properties at 77 K. Even though the films were grown under different conditions, the whole data set shows high J_c values. The differences in $J_c(B)$, particularly at low fields, can be explained by the different film thicknesses and microstructures as described in more detail below. In the mid-to-high field regime $B \geq 2$ T, all YBCO-BYNTO films show significantly higher J_c values, comparable with the best reference data for YBCO-BZO films, independent of growth conditions. Different from BZO artificial pinning centres, BYNTO nanocolumns grow highly oriented, straight and continuous along the whole film thickness in PLD-deposited YBCO films without the need for any fine tuning [20, 21].

In order to directly compare the potential of BZO and BYNTO as artificial pinning centres, in **Fig. 3** the $J_c(B)$ of YBCO-BZO and YBCO-BYNTO films grown at ENEA under optimised deposition conditions (considering J_c at 77 K and T_c) are compared at several temperatures.

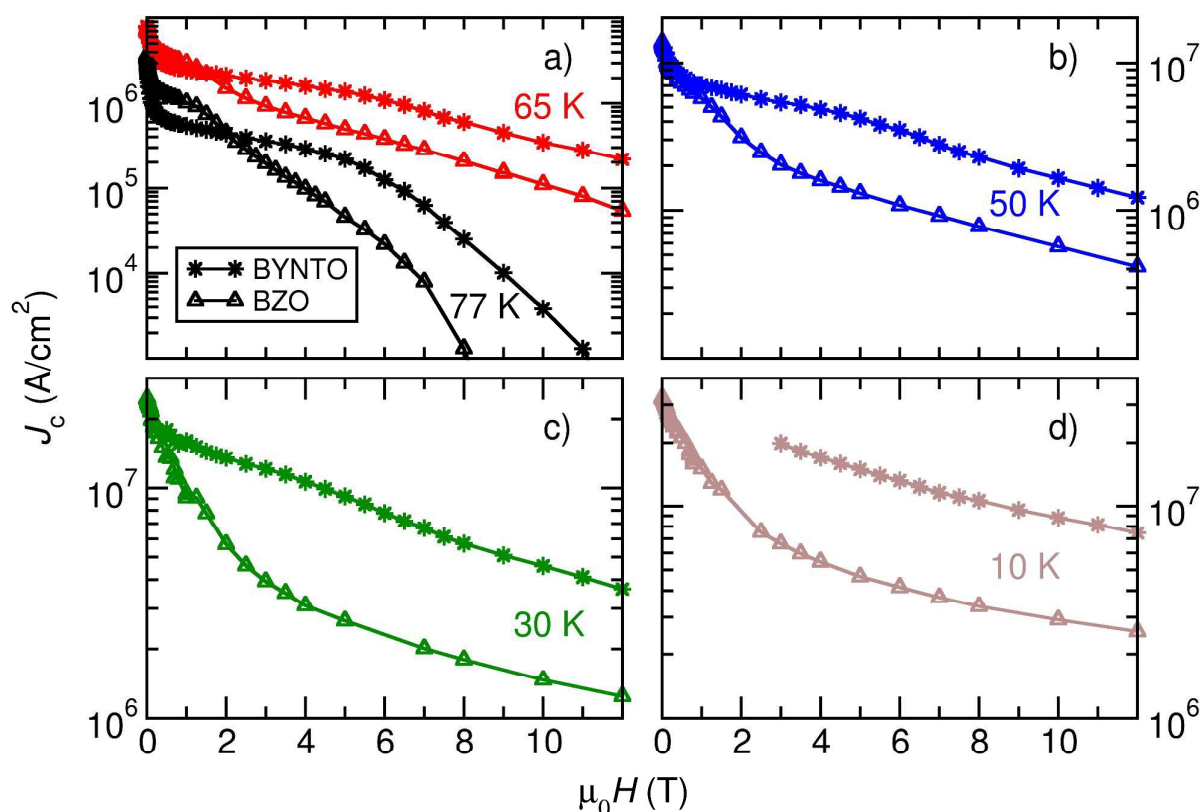


Figure 3: $J_c(B)$ comparison for ENEA YBCO-BYNTO (stars) and ENEA YBCO-BZO (triangles) in the temperature range [10-77] K. Both systems were grown under conditions optimized for J_c and T_c at 77 K.

At the relatively high temperatures of $T = 77$ K (black symbols) and $T = 65$ K (red symbols), YBCO-BZO exhibits a slightly higher J_c in the low-field regime $B < 2$ T, while YBCO-BYNTO shows a higher critical current density in the high-field region $B \geq 2$ T (**Fig. 3 a**). At lower temperatures, the low-field interval in which the YBCO-BZO J_c exceeds the YBCO-BYNTO J_c narrows. At the same time, the J_c high-field performance of YBCO-BYNTO improves with respect to YBCO-BZO. This behaviour sharpens more as the temperature decreases, as clearly shown in **Fig. 3 b-d**). Therefore, for YBCO films grown under optimised conditions (considering J_c at 77 K and T_c) with similar substrates and percentage of secondary phase addition, BYNTO additions result in more effective pinning centres with respect to BZO in the mid-to-high magnetic field range over the whole temperature interval explored. However, YBCO-BZO films with even better performances than shown in Fig. 3 can be found in the literature [30]. Consequently, the maximum pinning forces achievable with BYNTO nanocolumns may not have been reached yet and further improvement is expected for better fine tuning of the nanocolumn properties.

The angular dependence of J_c at 77 K and 1, 3 and 5 T is shown in **Fig. 4** for YBCO-BYNTO films grown at laser repetition rates of 1, 2 and 10 Hz, (IFW, UCAM, and ENEA respectively).

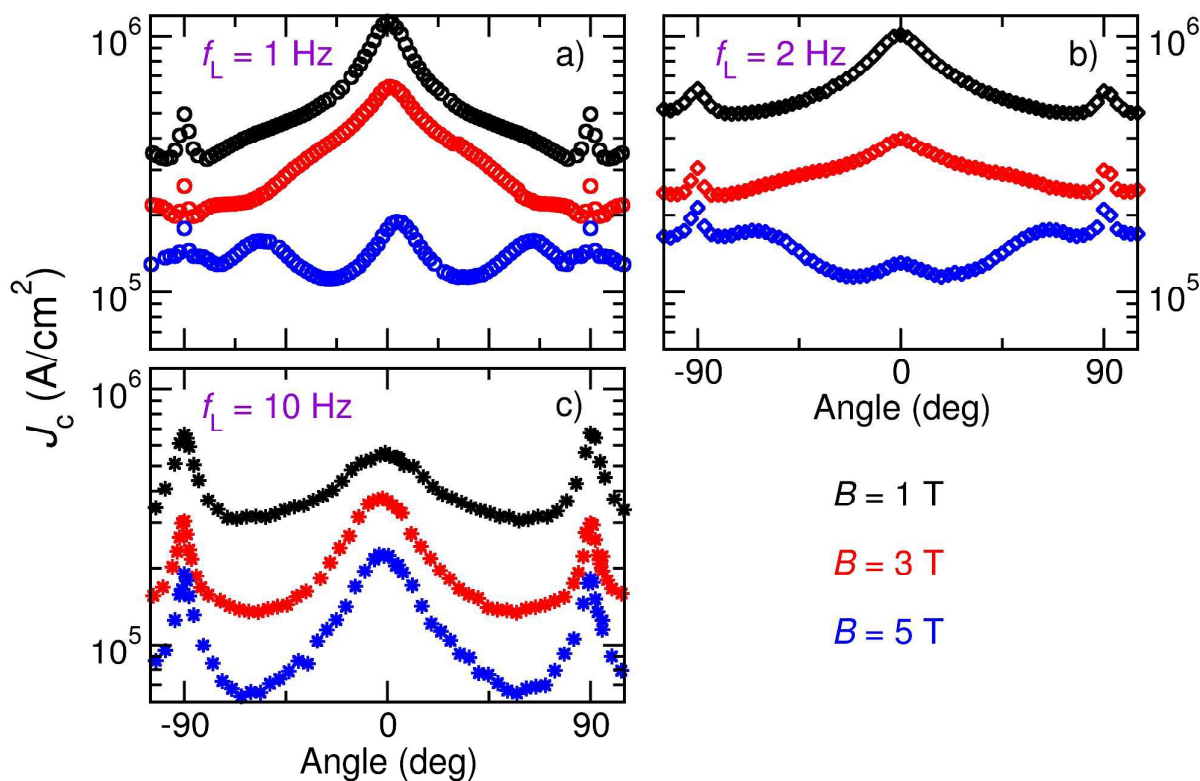


Figure 4: Influence of the laser repetition rate on the angular dependence of J_c at 77 K and applied field values 1 T, 3 T and 5 T. Zero degrees corresponds to the field orientation parallel to the YBCO c -axis.

A broad correlated peak at 0° ($B||c$) is clearly present for all YBCO-BYNT0 films, irrespective of the laser repetition rate. This peak is related to the continuous and straight BYNT0 columnar growth along the YBCO c -axis, as confirmed by the planar and cross-sectional TEM images shown below in **Fig. 5** and **Fig. 6**.

However, considerable differences arise in the angular behaviour. The films deposited at low repetition rates ($f_L = (1, 2)$ Hz) show a strong correlated contribution in the low-to-mid magnetic field range $B = [1 - 3]$ T. When the magnetic field is increased to 5 T, the correlated peak at 0° strongly reduces with respect to the 90° peak and secondary peaks appear at intermediate angles between 45° and 90° . Such peaks have been observed previously [19] and are ascribed to the presence of additional Y_2O_3 nanoparticles (see **Fig. 6 a**) and/or can be described by a matching effect of the magnetic field's c -axis component [20]. The Y_2O_3 particles grow parallel to the YBCO ab -plane and, acting as pinning structures in concurrence with BYNT0 nanocolumns, give rise to a staircase-like pinning landscape. The YBCO-BYNT0 film grown at a laser repetition rate of 10 Hz (Fig. 4 c)) does not show the intermediate-angle feature at any value of the magnetic field. In addition, at 1 T the correlated peak is less pronounced with respect to the samples grown with $f_L = 1$ Hz and 2 Hz. Nevertheless, this peak is still clearly evident in the intermediate-to-high field regime $B = (3, 5)$ T.

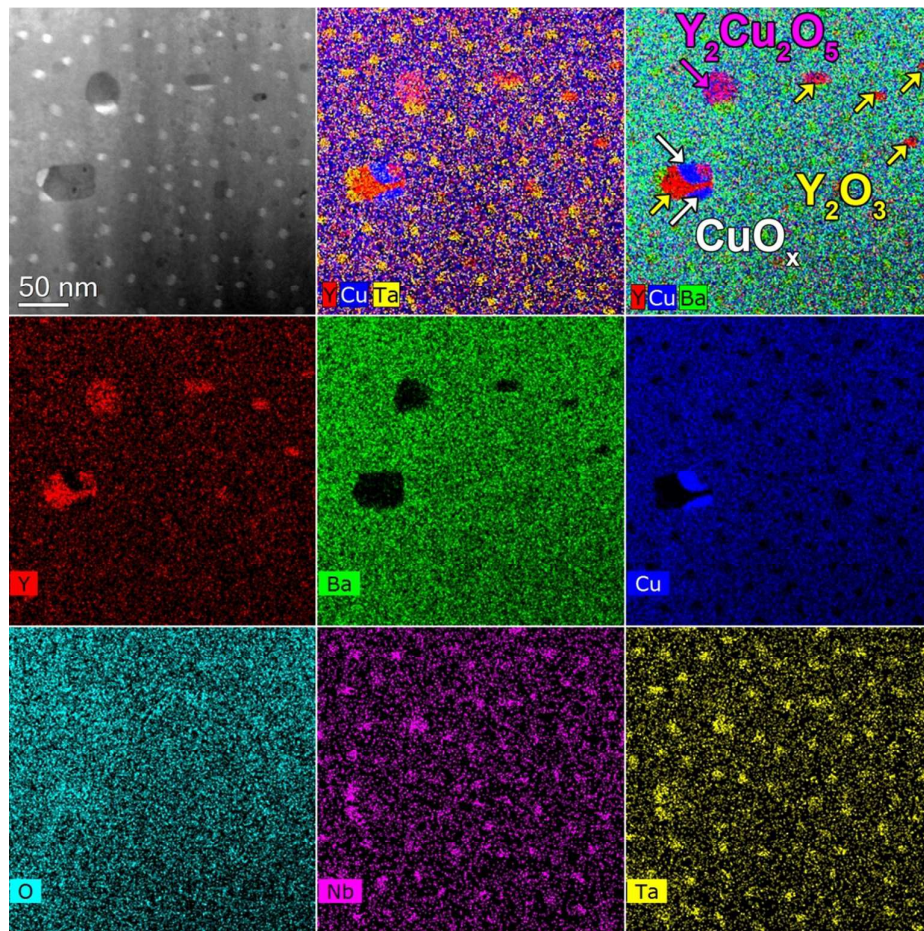


Figure 5: Plan view HAADF STEM image of a film grown at $f_L = 1$ Hz, with energy dispersive X-ray maps (EDX) showing the elemental composition. Homogeneously dispersed BYNTO columns intersecting the film plane are observed.

The results can be understood from the different sizes and density of the nanocolumns at the different growth rates: **Fig. 5** shows a plan-view HAADF image of the 1 Hz YBCO-BYNTO film in combination with the elemental composition identification. A very homogeneous distribution of the BYNTO nanocolumns is observed. The elemental maps also reveal the presence of some Y_2O_3 nanoparticles (roughly the same size as the nanocolumns) and occasionally a minor amount of $Y_2Cu_2O_5$ and CuO_x .

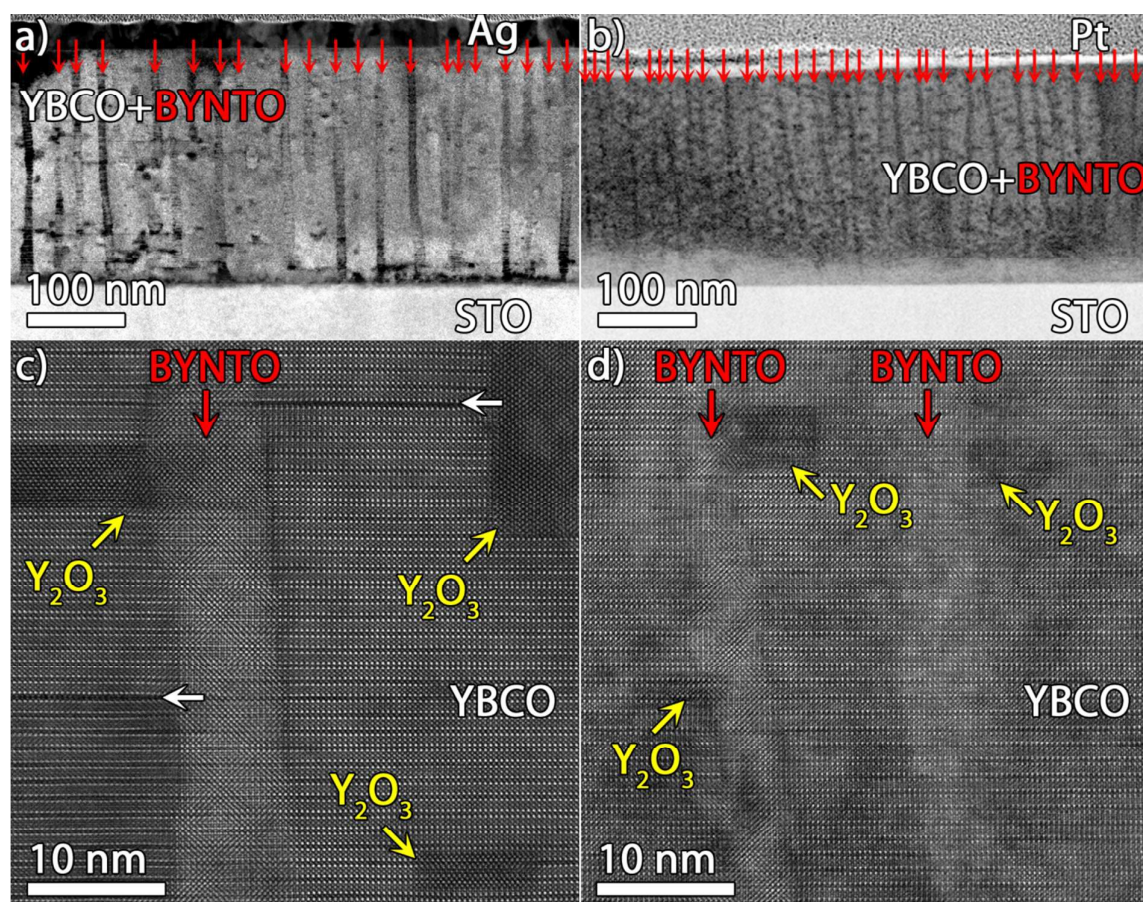


Figure 6: Cross-section overviews and high resolution HAADF STEM images of the 1 Hz (a, c) and 10 Hz (b, d) YBCO-BYNT0 films. BYNT0 columns are marked by red arrows. Note the higher density of columns in the 10 Hz sample. The samples are highly decorated by Y_2O_3 nanoparticles ($\sim 1-20$ nm). The white arrows indicate double CuO chain plane intergrowths in the YBCO matrix.

Fig. 6 compares the cross sectional TEM images of YBCO-BYNT0 films grown at $f_L = 1$ Hz (a, c) and $f_L = 10$ Hz (b, d). Both YBCO films present evidence of BYNT0 nanocolumnar structures, highlighted by the red arrows. The columns nucleate on a thin, highly distorted YBCO layer at the interface with the STO substrate (**Fig. 6** a, b)). The nanocolumns are continuous and extend over the whole film thickness. Y_2O_3 nanoparticles develop close to the BYNT0 nanocolumns as well as isolated in the YBCO matrix; they are highlighted by yellow arrows in **Fig. 6** c) and d). These nanoparticles contribute to the peculiar J_c angular behaviour shown in **Fig. 4** a) and b). The nanocolumn mean diameter for $f_L = 10$ Hz is $d_{10\text{Hz}} \sim 5$ nm, while for $f_L = 1$ Hz it is $d_{1\text{Hz}} \sim 9.6$ nm. A smaller mean diameter at the same doping level leads to a larger density of nanocolumns, $n_{10\text{Hz}} \sim 2500 \mu\text{m}^{-2}$ compared to $n_{1\text{Hz}} \sim 1040 \mu\text{m}^{-2}$ (**Fig. 6**).

The nanocolumn density and size depends on the growth rate, which in turn influences the kinetics of film growth and nanocolumn formation. Similar to the YBCO-BZO system [17], the

mechanism of nanocolumn formation is promoted by Ta and Nb ion diffusivity at the growing film surface. It is likely that the increased rate of species arrival, which affects the growth rate, would reduce the range of ion migration, i.e. the ion diffusivity. Reduced diffusivity leads to a larger density of columns with smaller diameter. In addition, nanocolumns in the $f_L = 10$ Hz case show a more splayed growth, in accordance with [16], where this effect was shown for varying deposition temperature, the other experimental parameter determining the diffusivity [17].

The structural differences evidenced by the TEM analysis coherently match with the angular transport properties shown in **Fig. 4**. Indeed, the straight nanocolumns in the YBCO-BYNT0 film grown at $f_L = 1$ Hz effectively pin c -axis oriented vortices up to a complete match between nanocolumns and vortices, which corresponds to a specific matching magnetic flux density value B_m [20]. Nevertheless, the pinning capability along the c -axis decreases above B_m due to the increased vortex density. Consistently, the correlated peak shows a strong intensity in the low-to-mid magnetic field range $B = [1-3]$ T and reduces with respect to the ab -peak at the intermediate field value of 5 T (see **Fig.4 a**). In the YBCO-BYNT0 film grown at $f_L = 10$ Hz, the more splayed BYNT0 nanocolumn distribution is less efficient in pinning the c -axis-oriented vortices for low values of the applied magnetic field. As a result, in the low magnetic field regime, $B = 1$ T, the correlated peak exhibits a moderate intensity with respect to the previous case. Going to the intermediate magnetic field regime $B = [3 - 5]$ T, the larger density of nanocolumns ($n_{10\text{Hz}} \sim 2.5 n_{1\text{Hz}}$) allows a more efficient arrangement of the vortices in the columnar pinning sites. In fact, an estimate of the inter-vortex spacing in the Abrikosov lattice $a = (2/\sqrt{3})^{1/2}(\phi_0/B)^{1/2}$ [31] (where ϕ_0 is the magnetic flux quantum) gives $a_{5\text{T}} \sim 22$ nm at $B = 5$ T. This value is lower than the inter-column distance $c_{1\text{Hz}} \sim 30$ nm in the film grown at $f_L = 1$ Hz. However, the inter-column distance for the film deposited at $f_L = 10$ Hz is $c_{10\text{Hz}} \sim 20$ nm. Hence, the BYNT0 nanocolumns distribution in the film grown at the higher laser repetition rate of $f_L = 10$ Hz can effectively trap c -axis oriented vortices in the intermediate field regime, resulting in a pronounced correlated peak in the J_c angular behaviour.

The dependencies of the column diameter as well as the matching field on the laser repetition rate are shown in **Fig. 7** for samples grown at the laser radiation wavelengths of 248 nm and 308 nm (IFW and ENEA samples respectively), illustrating the tunability of the BYNT0 nanocolumns in the YBCO matrix: the diameter of the columns linearly decreases by increasing the laser repetition rate, an external growth parameter easily set and controlled.

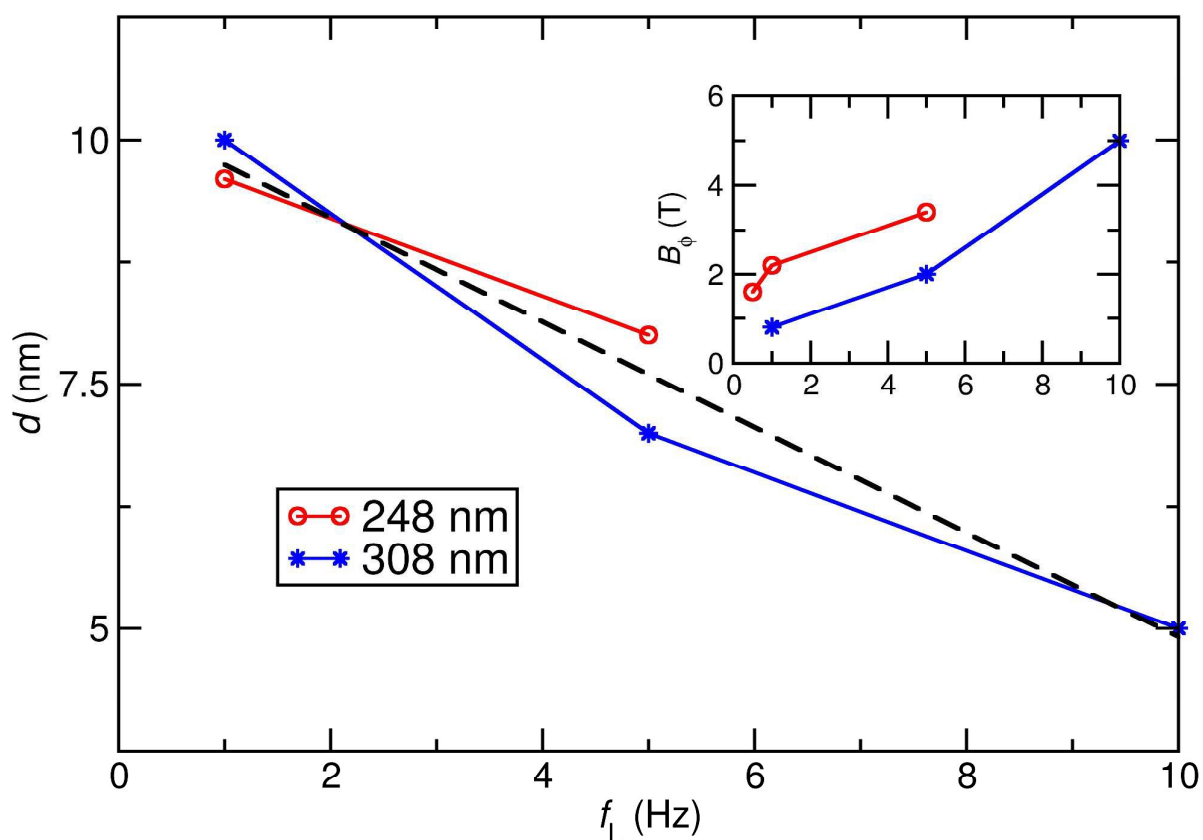


Figure 7: Experimental diameter of the nanocolumns as a function of the laser repetition rate (stars refer to $\nu_L = 308$ nm, circles refer to $\nu_L = 248$ nm) and corresponding linear fit (dashed line). The inset shows the behaviour of the matching field as a function of the laser repetition rate.

Also the density of nanocolumns, and hence the matching field value, shows a linear dependence with f_L . However in this case, having fixed the laser repetition rate, the density of columns increases by decreasing ν_L , hence by increasing the growth rate per pulse. This feature can be explained considering the reduced ion diffusivity at higher growth rate. As already discussed, this is consistent with a larger density of columns.

While the $J_c(B)$ and $J_c(\theta)$ data of **Figs. 1-4** altogether show the excellent in-field performance of YBCO-BYNT0 films across a wide temperature regime, deeper understanding of the effectiveness of BYNT0 nanocolumnar inclusions as strongly correlated pinning sources can be gained by analysing the J_c temperature dependence.

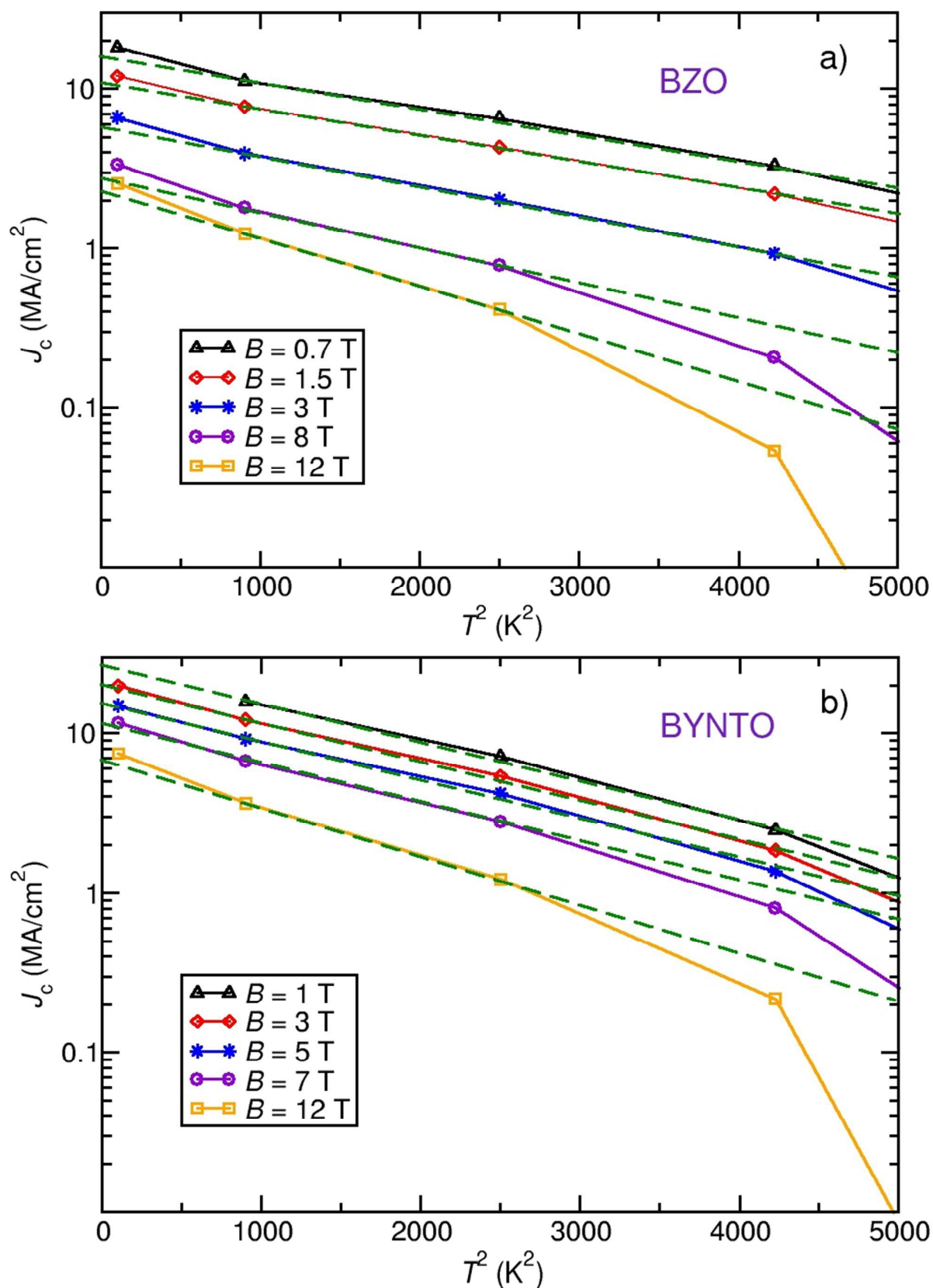


Figure 8: $J_c(T)$ on log scale vs T^2 at various magnetic fields values for YBCO-BZO (a) and YBCO-BYNT0 (b) films. Green dashed lines are data fits according to the empirical formula $J_c(T) \sim J_c(0)\exp(-3(T/T^*)^2)$.

Fig. 8 compares $J_c(T)$ of YBCO-BZO and YBCO-BYNT0 on a log scale vs T^2 . In the YBCO-BZO film (**Fig. 8 a**), an exponential decay with T^2 is noticeable in the temperature range $T \sim [30 - 65]$ K in the low-to-mid field range. By increasing the magnitude of the field, the upper limit of this range drops. This $J_c(T)$ behaviour is well fitted by the empirical expression $J_c(T) \sim J_c(0)\exp(-3(T/T^*)^2)$, in agreement with previous studies [5, 27], and shows that BZO nano-columns provide an effective strong pinning contribution down to ~ 30 K. At lower temperatures, $J_c(T)$ shows an upward deviation with respect to the fit extrapolation, indicating that an additional weak pinning contribution emerges and dominates in this temperature regime. Oxygen point defects created by local strain at YBCO-secondary phase interfaces in the films have been recently identified as excellent weak collective-pinning resulting in very high J_c [30]. Accordingly, this could be a mechanism contributing to the superior performance at low operating temperatures in our YBCO-BYNT0 films. On the other hand, a remarkably different behaviour is observed for YBCO-BYNT0 (**Fig. 8 b**). The empirical exponential decay $J_c(T) \sim J_c(0)\exp(-3(T/T^*)^2)$ as function of T^2 is observed in the whole low-to-mid temperature range explored [10 - 65] K and in the field range $B < B_m$. Furthermore, the $J_c(0)$ values are larger than for BZO for all applied fields. This means that the weak pinning contribution has a smaller fraction compared to the strongly one with respect to the YBCO-BZO case.

Additionally, the slope is the same for all the curves, indicating that T^* has a similar value for all fields. This value is lower than the corresponding one observed in BZO (the values estimated by fitting data are $T_{\text{BYNT0}}^* \sim 72$ K, $T_{\text{BZO}}^* \sim 82$ K). In fact, for fields below the matching field B_m^{BZO} , $J_c(T)^{\text{BZO}}$ shows a slower decay with temperature with respect to $J_c(T)^{\text{BYNT0}}$. For magnetic fields above the matching field B_m , $J_c(T)$ shows a crossover toward the trend observed in YBCO-BZO films with the upward deviation. This analysis definitely shows that, differently from BZO, BYNT0 nanocolumns together with Y_2O_3 nanoparticles provide a microstructural landscape with a strong correlated pinning mechanism which is active, for field magnitudes up to B_m , down to the low temperature regime.

Conclusions

Highly effective pinning to high fields, up to 12 T of applied magnetic field, was demonstrated across the whole temperature regime, from 10 K to 77 K, in YBCO conductors. Remarkable J_c values were obtained across the (10 - 77) K temperature and (0 - 12) T field regime. This was done by engineering $\text{Ba}_2\text{Y}(\text{Nb,Ta})\text{O}_6$ nanocolumnar inclusions into YBCO films under different conditions of temperature, growth rate and composition in different laboratories. Remarkably

similar J_c versus $H \parallel c$ transport properties were obtained for the different films, with fine variations consistent with micro-structural differences highlighted by TEM analysis. This lack of need for tight composition and processing control is very beneficial and indeed necessary for future industrial production of coated conductors. In addition, tuning of the nanocolumn growth diameter and density and hence the pinning behaviour was readily possible by using different film growth rates.

In particular, much improved performance was achieved in the low temperature regime down to 10 K. J_c values were greater than 10 MA/cm² for fields near 10 T at 10 K, and the corresponding pinning force density was ~ 1 TN/m³. This remarkable performance was obtained at a relatively low BYNTO doping level (5 mol.%). Greater improvements are expected at higher doping content.

Analysis of the temperature dependence of the critical current density at several magnetic field values revealed an unexpected low-temperature feature. Contrary to YBCO-BZO, the strong pinning linked to the peculiar YBCO-BYNTO microstructural landscape remains active to 10 K and up to the matching field B_m .

Finally, YBa₂Cu₃O_{7-x} films with Ba₂Y(Nb,Ta)O₆ inclusions represent a robust and very promising system for the development of coated conductors in applications requiring mid to high fields across a broad range of temperatures.

Methods

Film deposition

Epitaxial (00 l) YBCO films with self-assembled BYNTO nanocolumns have been grown on commercially available SrTiO₃ (STO) single crystals by means of pulsed laser deposition (PLD). The PLD targets were sintered by mixing and grinding pure YBCO powder and single-phase BYNO and BYTO powders in the ratios of either 50:50 (ENEA, Institut für Festkörper- und Werkstoffforschung (IFW) or 75:25 (University of Cambridge, UCAM). The 75:25 composition is shown for UCAM data as a slightly improved performance was obtained compared to 50:50 in the UCAM lab. The 75:25 composition was not explored in the other labs. The overall level of secondary phase additions to the YBCO powder was 5 mol.%. Further details on target preparation can be found in Ref. [19]. Thin films have been grown in three different PLD systems at ENEA, UCAM and IFW. Depending on the PLD system, the deposition has been achieved using a XeCl laser (wavelength $\lambda_L = 308$ nm), adopted by ENEA, or a KrF laser (wavelength $\lambda_L = 248$ nm), adopted by UCAM and IFW, in the repetition rate range $f_L = [1$

- 10] Hz, with a fluence of about 2.0 J/cm². The film thickness ranged from 220 nm to 500 nm as confirmed by TEM cross-sectional analyses.

Structural Characterization

All the samples reported in this work exhibit a high degree of epitaxy for both the YBCO matrix and the BYNTO inclusions as revealed by X-ray diffraction measurements [20, 21]. Typical values of the ω -scan full width at half maximum for the (005) YBCO peak are less than 0.3°, indicating a high degree of *c*-axis alignment. The crystallographic relationships [100]_{YBCO}||[100]_{BYNTO} and [001]_{YBCO}||[001]_{BYNTO} are found.

TEM cross-sectional analyses were used to study BYNTO nano-inclusions in the YBCO matrix and to estimate their physical properties (average size, density, linearity and distribution). Samples for transmission electron microscopy (TEM) were prepared by Focused Ion Beam (FIB, FEI Helios Nanolab 600i). High angle annular dark field scanning transmission electron microscopy (HAADF-STEM) and energy dispersive X-ray spectroscopy (EDX) were performed on a FEI Titan “cubed” and FEI Osiris electron microscopes equipped with a “Super-X” wide solid angle EDX detector and operated at 200 kV. Before TEM analysis, all samples were plasma cleaned.

Electrical transport measurements

The samples were processed with a standard U.V. photolithographic and wet etching method in order to obtain 30-50 μm wide and 0.8-1 mm long strips for J_c measurements. Gold contacts were deposited on sputtered current/voltage pads with a lift-off technique and e-beam evaporator to improve the electrical contact quality. The films have been mounted in a He-flow cryostat provided with a 12 T superconducting magnet (ENEA) or in physical property measurement systems up to 9 T (IFW, UCAM) in order to measure the transport properties as a function of temperature and applied field. A rotating probe has been used to measure the J_c magnetic field orientation dependence, while always keeping the current normal to the field direction (maximum Lorentz force configuration). All the measurements were performed using a standard four-point probe configuration with a 1 μV/cm electric field criterion.

Conflicts of interest

There are no conflicts of interest to declare

Acknowledgements

This work was partially financially supported by EUROTAPES, a collaborative project funded by the European Commission's Seventh Framework Program (FP7/2007-2013) under Grant Agreement No. 280432.

This work has been partially carried out within the framework of the EUROfusion Consortium and has received funding from the Euratom research and training programme 2014-2018 under grant agreement No 633053. The views and opinions expressed herein do not necessarily reflect those of the European Commission.

Author Contributions

F.R. deposited the samples, performed the transport properties measurements, designed the experiment and prepared the manuscript. A.A. performed the transport properties measurements and prepared the manuscript. J.L.M.D. had input on the composition design and manuscript writing. A.K. prepared the PLD targets, deposited the samples and performed the transport properties measurements. M.B. prepared the PLD targets, deposited the samples and performed the transport properties measurements. L.O. deposited the samples and performed the transport properties measurements. M.S. deposited the samples and performed the transport properties measurements. R.H. designed the experiment. J.H. designed the experiment and contributed to the manuscript preparation. A.M. conducted the TEM analysis. G.V.T. conducted the TEM analysis. G.C. designed the experiment and prepared the manuscript. All authors took part in analysis of the results and commented on the manuscript.

Additional Information

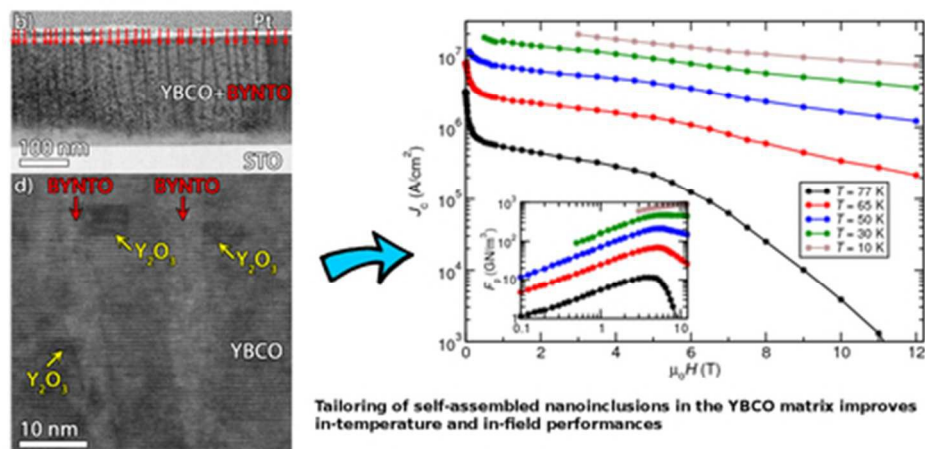
Corresponding author: Correspondence to francesco.rizzo@enea.it

References

- [1] Obradors, X., Puig, T. Coated conductors for power applications: materials challenges. *Supercond. Sci. Technol.* **27**, 044003 (2014).
- [2] Takao, Y., Awano, M., Takagi, H. Preparation and Properties of $\text{Ba}_2\text{YCu}_3\text{O}_{7-x}\text{-BaZrO}_3$ Superconductive Composite by Spray Drying Method. *Journal of Ceramic Society of Japan* **102**, Issue 3, 237-240 (1994).
- [3] J. L. MacManus-Driscoll, J. L. *et al.* *Nature Mater.* **4**, 439-443 (2004).
- [4] Goyal, A. *et al.* Irradiation-free, columnar defects comprised of self-assembled nanodots and nanorods resulting in strongly enhanced flux-pinning in $\text{YBa}_2\text{Cu}_3\text{O}_{7-\delta}$ films. *Supercond. Sci. Technol.* **18**, 1533-1538 (2005).
- [5] Gutiérrez, J. *et al.* Strong isotropic flux pinning in solution-derived $\text{YBa}_2\text{Cu}_3\text{O}_{7-x}$ nanocomposite superconductor films. *Nature Mater.* **6**, 367-373 (2007).
- [6] K. Matsumoto, K., Mele, P. Artificial pinning center technology to enhance vortex pinning in YBCO coated conductors. *Supercond. Sci. Technol.* **23**, 014001 (2010).

- [7] Tixador, P. Development of superconducting power devices in Europe. *Physica C* **470**, 971–979 (2010).
- [8] M. Noe, M., Steurer, M. High-temperature superconductor fault current limiters: concepts, applications, and development status. *Supercond. Sci. Technol.* **20**, R15–R29 (2007).
- [9] Muzzi, L., De Marzi, G., Di Zenobio, A., della Corte, A. Cable-in-conduit conductors: lessons from the recent past for future developments with low and high temperature superconductors. *Supercond. Sci. Technol.* **28**, 053001 (2015).
- [10] Harrington, S. A. *et al.* Self-assembled, rare earth tantalate pyrochlore nanoparticles for superior flux pinning in $\text{YBa}_2\text{Cu}_3\text{O}_{7-\delta}$ films. *Supercond. Sci. Technol.* **22**, 022001 (2009).
- [11] Wee, S. H. *et al.* Phase Stability of Pyrochlore Rare Earth Tantalate Pinning Additives in $\text{YBa}_2\text{Cu}_3\text{O}_{7-\delta}$ Superconductor. *J. Am. Ceram. Soc.* **95** [4], 1174–1177 (2012).
- [12] Wee, S. H. *et al.* Enhanced flux pinning and critical current density via incorporation of self-assembled rare-earth barium tantalate nanocolumns within $\text{YBa}_2\text{Cu}_3\text{O}_{7-\delta}$ films. *Phys. Rev. B* **81**, 140503(R) (2010).
- [13] Wee, S. H. *et al.* Formation of Self-Assembled, Double-Perovskite, Ba_2YNbO_6 Nanocolumns and Their Contribution to Flux-Pinning and J_c in Nb-Doped $\text{YBa}_2\text{Cu}_3\text{O}_{7-\delta}$ Films. *Appl. Phys. Express* **3**, 023101 (2010).
- [14] Feldmann, D. M. *et al.* Improved flux pinning in $\text{YBa}_2\text{Cu}_3\text{O}_7$ with nanorods of the double perovskite Ba_2YNbO_6 . *Supercond. Sci. Technol.* **23**, 095004 (2010).
- [15] Ercolano, G., Harrington, S. A., Wang, H., Tsai, C. F., MacManus-Driscoll, J. L. Enhanced flux pinning in $\text{YBa}_2\text{Cu}_3\text{O}_{7-\delta}$ thin films using Nb-based double perovskite additions. *Supercond. Sci. Technol.* **23**, 022003 (2010).
- [16] Maiorov, B. *et al.* Synergetic combination of different types of defect to optimize pinning landscape using BaZrO_3 -doped $\text{YBa}_2\text{Cu}_3\text{O}_7$. *Nat. Mater.* **8**, 398 (2009).
- [17] Wu, J. Z. *et al.* The effect of lattice strain on the diameter of BaZrO_3 nanorods in epitaxial in epitaxial $\text{YBa}_2\text{Cu}_3\text{O}_{7-\delta}$ films. *Supercond. Sci. Technol.* **27**, 044010 (2014).
- [18] Pahlke, P. *et al.* Reduced J_c anisotropy and enhanced in-field performance of thick BaHfO_3 -doped $\text{YBa}_2\text{Cu}_3\text{O}_{7-\delta}$ films on ABAD-YSZ templates. *IEEE Transactions on Applied Superconductivity* **26**, 6603104, 1–4 (2016).
- [19] Ercolano, G. *et al.* State-of-the-art flux pinning in $\text{YBa}_2\text{Cu}_3\text{O}_{7-\delta}$ by the creation of highly linear, segmented nanorods of $\text{Ba}_2(\text{Y/Gd})(\text{Nb/Ta})\text{O}_6$ together with nanoparticles of $(\text{Y/Gd})_2\text{O}_3$ and $(\text{Y/Gd})\text{Ba}_2\text{Cu}_4\text{O}_8$. *Supercond. Sci. Technol.* **24**, 095012 (2011).
- [20] Opherden, L. *et al.* Large pinning forces and matching effects in $\text{YBa}_2\text{Cu}_3\text{O}_{7-\delta}$ thin films with $\text{Ba}_2\text{Y}(\text{Nb/Ta})\text{O}_6$ nano-precipitates. *Sci. Rep.* **6**, 21188.
- [21] Rizzo, F. *et al.* Enhanced 77 K vortex-pinning in $\text{YBa}_2\text{Cu}_3\text{O}_{7-x}$ films with Ba_2YTaO_6 and mixed $\text{Ba}_2\text{YTaO}_6 + \text{Ba}_2\text{YNbO}_6$ nano-columnar inclusions with irreversibility field to 11 T, *APL Mater.* **4**, 061101 (2016).
- [22] Baca, J. F. *et al.* Interactive growth effects of rare-earth nanoparticles on nanorod formation in $\text{YBa}_2\text{Cu}_3\text{O}_{7-\delta}$ thin films. *Adv. Funct. Mater.* **23**, 4826–4831 (2013).
- [23] Singh, R. K. and Kumar, D. Pulsed Laser Deposition and Characterization of High- T_c $\text{YBa}_2\text{Cu}_3\text{O}_{7-x}$ Superconducting Thin Films. *Materials Science and Engineering: R: Reports* **22**, 113–185. 10.1016/S0927-796X(97)00019-3.
- [24] Kang, S. *et al.* High-performance high- T_c superconducting wires. *Science* **311**, 1911–1914 (2006).
- [25] Mele, P. *et al.* Ultra-high flux pinning properties of BaMO_3 -doped $\text{YBa}_2\text{Cu}_3\text{O}_{7-x}$ thin films ($M = \text{Zr}, \text{Sn}$). *Supercond. Sci. Technol.* **21**, 032002 (2008).
- [26] Augieri, A. *et al.* Pinning analyses on epitaxial $\text{YBa}_2\text{Cu}_3\text{O}_{7-x}$ films with BaZrO_3 inclusions. *J. Appl. Phys.* **108**, 063906 (2010).
- [27] Selvamanickam, V. *et al.* High critical currents in heavily doped $(\text{Gd,Y})\text{Ba}_2\text{Cu}_3\text{O}_x$ superconductor tapes. *Appl. Phys. Lett.* **106**, 032601 (2015).

- [28] Xu, A., Braccini, V., Jaroszynski, J., Xin, Y., Larbalestier, D. C. Role of weak uncorrelated pinning introduced by BaZrO₃ nanorods at low-temperature in (Y,Gd)Ba₂Cu₂O₇ thin films. *Phys. Rev. B* **86**, 115416 (2012).
- [29] Xu, A. *et al.* Strongly enhanced vortex pinning from 4 to 77 K in magnetic fields up to 31 T in 15 mol.% Zr-added (Gd, Y)-Ba-Cu-O superconducting tapes. *APL Materials* **2**, 046111 (2014).
- [30] Goyal, A., Wee S., H. Optimal, Nanodefekt Configuration via Strain-Mediated Assembly for Optimized Vortex-Pinning in Superconducting Wires from 5K-77K. *J. Phys.: Conf. Ser.* **871**, 012039 (2017).
- [31] Blatter, G., Feigelman, M. V., Geshkenbein, V. B., Larkin, A. I., Vinokur, V. M. Vortices in high-temperature superconductors. *Rev. Mod. Phys.* **66**, 1125–1388 (1994).



39x19mm (300 x 300 DPI)